Rotating Group Design for Vane Pump Flow Ripple Reduction

Leonardo Zanetti-Rocha and Samir N.Y. Gerges

Department of Mechanical Engineering, Federal University of Santa Catarina, University Campus, Trindade, 88040-900, Florianpolis-SC, Brazil

D. Nigel Johnston

Department of Mechanical Engineering, University of Bath, Bath, BA2 7AY, UK

Jorge P. Arenas

Institute of Acoustics, University Austral of Chile, PO Box 567, Valdivia, Chile

(Received 12 November 2012; accepted 20 August 2013)

It is well known that the hydraulic pump is the main source of noise in hydraulic power steering systems. This noise is produced by the pulsating flow transmitted through the fluid due to the cyclic pumping mechanism. This flow ripple and pressure ripple spread through the hydraulic circuit, interacting in a complex way with other parts of the vehicle. This process generates annoying audible noise inside the vehicle. This work addresses a new approach to flow ripple reduction by tuning the pump rotating group. The method consists of making the outlet flow as steady as possible by modifying the rotating group geometry. A MATLAB/Simulink-based pump model has been created according to the new geometrical characteristics and their numerical results, compared to the regular pump ones. In addition, a flow ripple experiment was conducted using the secondary source method (SSM to validate the numerically-predicted results of the regular pump. The results of the new design show significant amplitude reduction of the flow ripple amplitudes at different operating conditions. In particular, the flow ripple reduction at the first harmonic is almost 20 dB when the pump runs in a parking manoeuvres operating condition (1000 rpm at 50 bar of backpressure).

1. INTRODUCTION

Noise produced by the hydraulic power steering pump when operating a car can, in some situations, be perceived inside the vehicle as an annoying sound. The flow variations (flow ripple) generated by the pump through its natural operating process are transmitted along the power steering hydraulic circuit, interacting with the impedance of the hoses and tubes. This process generates structural vibration and, consequently, sound emission around the circuit.[1]

In some vehicles, the hydraulic circuit is tuned in order to avoid hearing noise inside the cabin. Flexible hoses, sometimes with tuning cables, are usually used to increase circuit compliance in order to remove unwanted resonance frequencies or reduce the flow ripple amplitude. In fact, there are several techniques and devices—such as silencers, side branches, accumulators, etc.—that can be used to reduce fluid-borne noise along the propagation circuit.[2,3]

However, if a pump can be manufactured with a lower noise profile, this may create a solution that is independent of the hydraulic circuit and does not require costly and time-consuming tuning of the system to achieve the required noise reduction.

The present work is aimed at vane pumps and proposes a new rotating group design, intended to reduce the flow ripple amplitude. Because this new design is not dependent on the number of vanes, an eight vane rotating group was developed to combine cost reduction with flow ripple reduction.

In order to achieve those results, a MATLAB/Simulink-based numerical model was created from a regular pump design and validated through the experimental secondary source mMethod (SSM), which has been developed at the University of Bath.[4,5] The SSM has been used as the basis for an international standard to measure pump pressure ripple characteristics.[6] The simulated results of the new design are compared here with the regular pump ones. A comparison is then made in terms of the flow ripple amplitudes in the frequency domain.

2. REGULAR PUMP CHARACTERISTICS

The regular automotive pump has two discharge ports located diametrically opposite to each other, i.e., they are spaced by an angle of 180° regarding the centre of the thrust plate as the centre of the reference circumference. This type of positive-displacement pump is called a *balanced pump* because these two opposite ports balance the forces acting against the rotor, and all the walls of the chamber as well, reducing the shaft pump oscillations and overall vibrations. Figure 1 shows the rotating group components and its assembly scheme.

The pump uses the engine torque applied to its shaft to pump oil from the inlet port to the outlet port. Figure 2 shows a scheme of the pumping process inside the pump. The system back pressure varies according to the outlet hydraulic circuit constraint, increasing the pressure as the constraint increases.

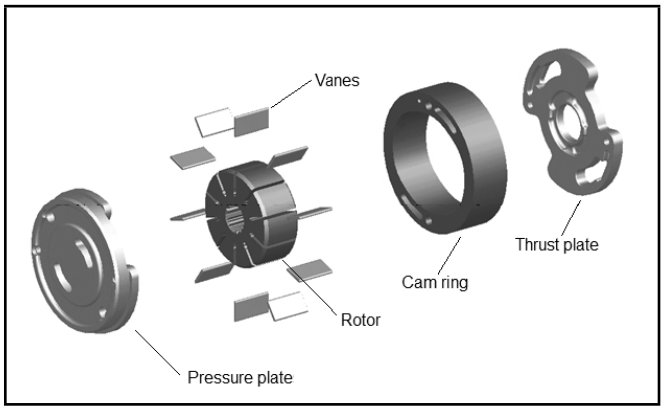

Figure 1. The rotating group components.

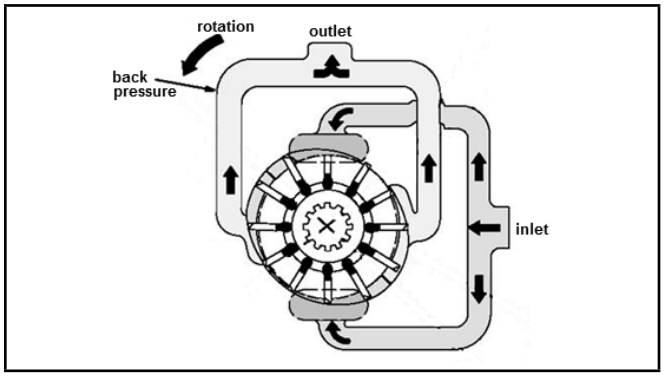

Figure 2. Schematics of the rotating group operation.

3. PUMP MODEL

The numerical model of the pump is based on the general continuity equation, choosing the chamber, between a leading vane and its trailing vane, as the control volume. Similar models have been developed by other authors.[7–9]

All the dimensions (geometric data) were loaded into the model from the drawings of a regular ten-vane automotive hydraulic pump. The rate of change of pressure with respect to time is given by

$$\frac{dp}{dt} = -\frac{\beta_e}{V}\frac{dV}{dt} - Q_{IN} - Q_{OUT} - Q_{LEAK}; \qquad (1)$$

where Q_{IN} is the flow in the inlet port, Q_{OUT} is the flow in the discharge port, β_e is the effective bulk modulus, V is the chamber volume, and Q_{LEAK} is the flow resulting from the leakage path inside the pump.

The flows through the inlet and outlet ports are calculated using the orifice equation, which relates the pressure difference between the downstream and upstream sides of a restriction. This is given by

$$Q = C_d A\sqrt{\frac{2\Delta p}{\rho}}; \qquad (2)$$

where C_d is the orifice flow coefficient, A is the orifice area, ρ is the fluid density, and Δp is the pressure difference between the upstream and downstream sides. The flow leakages are calculated using the equation for laminar leakage flow between two planes, one of which is moving relative to the other, i.e.,

$$Q_{LEAK} = \frac{LH^3(p-p_a)}{12\mu t_h} \pm \frac{vLh}{2}; \qquad (3)$$

where h is the clearance, L is the width of the gap, t_h is the length of the gap, μ is the fluid viscosity and v is the velocity. The first term on the right hand side of Eq. (3) describes the flow through the areas when both are fixed. The second term adds the effect of relative movement of the plates (Couette Flow).

Analysing the pump operation and the way that the internal parts are assembled, several leakage paths can be identified where leakage flows can be calculated. Therefore, Eq. (3) is used to calculate the following leakage paths into the pump rotating group.

1. Vane tip leakage:

$$Q_{vtl} = \frac{L_v h_1^3(p-p_a)}{12\mu t} \pm \frac{\omega r L_v h_1}{2}. \qquad (4)$$

2. Vane end leakage:

$$Q_{vll} = \frac{(r_c - r_r)h_2^3(p-p_a)}{12\mu t_v} \pm \frac{\omega(r_c+r_r)(r_c-r_r)h_2}{4}. \qquad (5)$$

3. Vane slot leakage:

$$Q_{vsl} = \frac{L_v h_3^3(p-p_{out})}{12\mu\left[h_v-(r_c-r_r)\right]}. \qquad (6)$$

In Eqs. (4)–(6), L_v is the vane length, h_1 is the vane tip clearance, h_2 is the vane end clearance, h_3 is the vane slot clearance, ω is the rotational speed of the vanes, p is the fluid chamber pressure, p_a is the adjacent (leading or trailing) fluid chamber pressure, h_v is the vane height, r_c is the radius of the cam ring from the centre of the rotor, and r_r is the rotor radius.

Figure 3 shows a scheme of a fluid chamber showing the three leakage paths corresponding to Eqs. (4)–(6). The scheme also shows a leakage path across the end faces of the rotor, q_{rli}, which is not included in the present model since its value is negligible.

The model also needs to include the 'under-vane' flow to the chambers at the inner radial faces of the vanes, caused by the vane movement which is expressed by

$$Q_{uv_i} = v_i L_v t_v; \qquad (7)$$

where $v_i = dr_i/dt$ is the radial speed of the vane. These chambers connect to the delivery port, and the pressure helps the vane with its radial movement to maintain contact against the ring wall, along with centrifugal forces. The sum of the under-vane flows results in the total pump under-vane flow, given by

$$Q_{uv} = \sum_{i=1}^{N_v} Q_{uv_i}; \qquad (8)$$

where N_v is the number of pump vanes (notice that in the standard pump, $N_v = 10$).

Some of the values used in the numerical simulation are presented in Table 1. The fluid bulk modulus is reduced to allow for the effect of air bubbles and compliance of the rotor and vanes. The vane end clearance was estimated from the vane

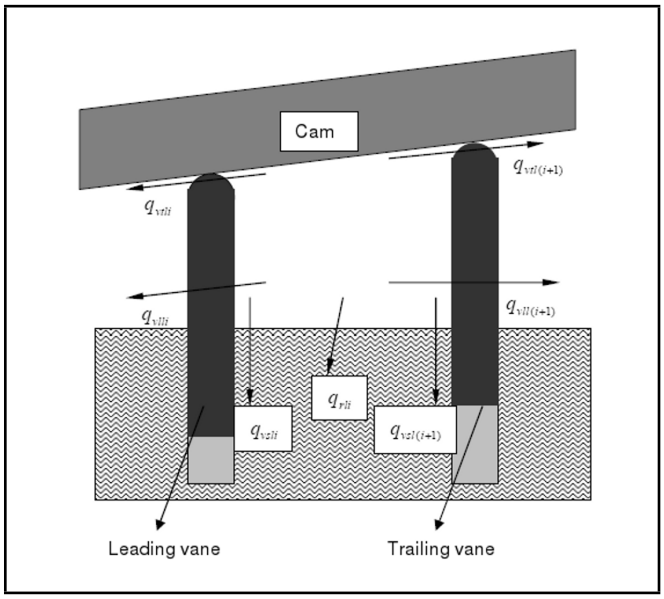

Figure 3. The leakage flows in and out of the fluid chamber.[8]

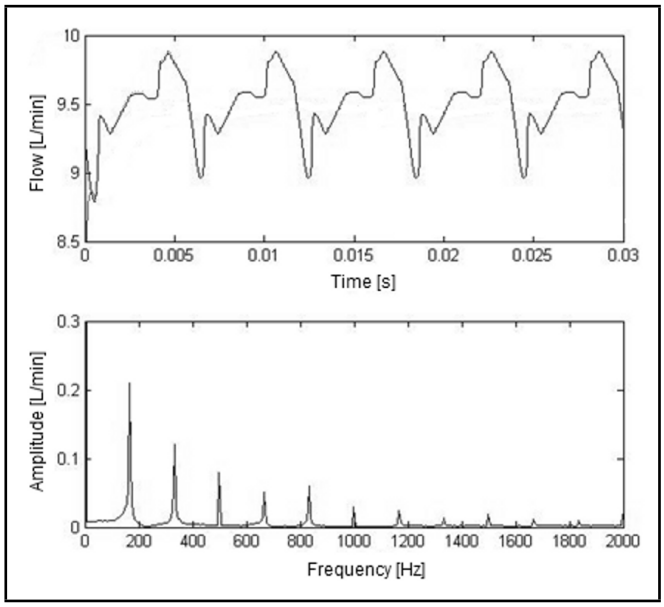

Figure 4. The regular pump outlet flow ripples (1000 rpm at 50bar).

Table 1. Values used in the numerical simulation.

Fluid viscosity	8.3 cP
Fluid density	870 kg/m^3
Effective bulk modulus	4×10^8 Pa
Flow coefficient for ports	0.6
Vane tip clearance	0.01 mm
Vane end clearance	0.019 mm
Vane slot clearance	0.01 mm
Rotor radius	20.7 mm
Rotor width	16 mm

and rotor dimensions. The vane tip and vane slot clearances are simple estimates, and in practice these clearances would be expected to vary as the vanes move through their cycle.

Figure 4 shows the regular pump numerical simulation, running at 1000 rpm at 50 bar.

4. SECONDARY SOURCE METHOD

The secondary source method (SSM), developed at the University of Bath,[4,5,10] was used in this work for measuring both the pump flow ripple and the impedance. The SSM was first adopted as the British Standard for measuring pump fluid-borne noise,[11] and was later used as the basis for an ISO standard in the measurement of pump pressure ripple characteristics.[6]

The SSM is based on the measurements of the harmonics of the pressure ripple at a series of points along the length of a rigid pipe connected either to the delivery or suction port of the test pump. The pressure ripple that occurs at two or three positions is analyszed to determine the pressure ripple.

From the Norton model, shown in Fig. 5, it is possible to find an equation to establish the flow ripple at the pump discharge port:

$$Q_0 = Q_s - \frac{P_0}{Z_s}; \tag{9}$$

where Q_s is the internal source flow, Q_0 is the flow ripple at the pump discharge port, P_0 is the pressure ripple at the discharge

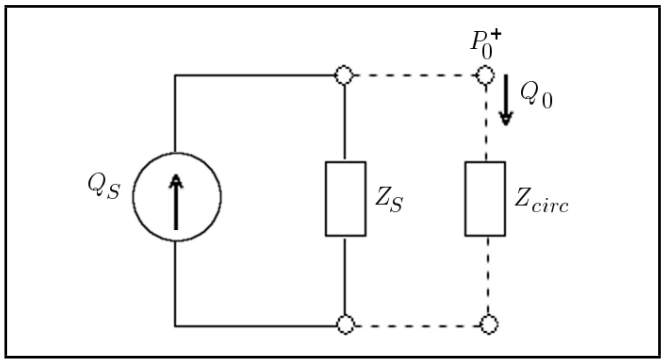

Figure 5. The Norton model of a pump.

port, and Z_s is the source impedance.

In order to calculate the source impedance, a secondary source of pressure ripple is placed downstream of the pump, as shown in Fig. 6. In this condition, the secondary source is operated at a different speed than the test pump and the harmonic components of this secondary source are measured. It can be shown that if the second pump flow ripple frequencies do not coincide with the pump under the test circumstances, the harmonic frequencies and the spectral leakages are negligible, while Q_s can be assumed to be zero. Therefore, the calculation of the source impedance Z_s can be separated from the calculation of the source flow ripple Q_s. Thus, Eq. (9) is simplified and the source impedance can be determined as

$$Z_s = -\frac{P_0}{Q_0}. \tag{10}$$

Measurements of the pressure ripple are then taken with the secondary source not operational, from which Q_s can be easily calculated through the Norton model, given that the values of Z_s, P_0 and Q_0 are known.

Even though the basic principles of SSM are presented, it is not the aim of this paper to discuss the method in detail. More information and the detailed evaluation of the SSM can be found in the literature.[4,5,10]

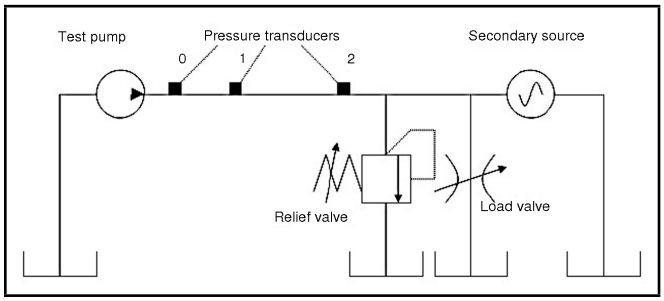

Figure 6. The hydraulic circuit for secondary source method.[12]

The simulated results were compared with the experimental ones measured through the SSM, and some results are shown in Fig. 7. The simulated results show reasonably good agreement with those obtained by the SSM when the pump is run at low speed—i.e., 1000 rpm in Fig. 7a and 7b. However, for more extreme conditions, e.g, 2000 rpm and 75 bar in Fig. 7c, the shape of the flow does not match accurately with the simulated ones.

To improve the experimental analysis, a frequency domain analysis was carried out. Figures 8a–8c show the simulated and measured results in the frequency domain of the outlet flow ripple for the same operating conditions considered in Figs. 7a–7c. It can be seen that when the pump is run at low speed, there is a good agreement between the measured and simulated results of amplitude of the first harmonics, where differences between the results vary from none to a maximum of 7 dB. On the other hand, Fig. 8 also shows a low correlation between measured and simulated amplitudes when the pump is run at high speeds, mainly at high frequencies, which explains the differences observed in Fig. 7c.

Differences between experimental and simulated results may be attributed to inaccuracies in the SSM, as well as simplifications and assumptions made in the simulation model. Uncertainties in the nature of the delivery passageway and the integral flow control valve, which are not included in the model, may explain some of the differences. Nonetheless, the similarity in the amplitude and the trends of the results in the time-domain analysis, and the similarity in the amplitudes of the first harmonics in the frequency-domain analysis, indicate that the results obtained from the simulation model are reasonable and may be used to investigate the effect of making changes in the design of the rotor, cam and ports.

5. REGULAR PUMP FLOW RIPPLE ANALYSIS

As seen previously, the pump outlet flow ripple is the result of several hydraulic phenomena that occur inside the rotating group during the operation. To understand how the outlet flow ripple is formed, it is important to analyse the influence of each one of these phenomena separately. Once this analysis is done, it would be possible to act over each phenomenon in order to reduce the flow ripple amplitude.

5.1. Timing Analysis

Figure 9 shows the simulated outlet flow without the influence of the internal leakage flows and the under-vane flows,

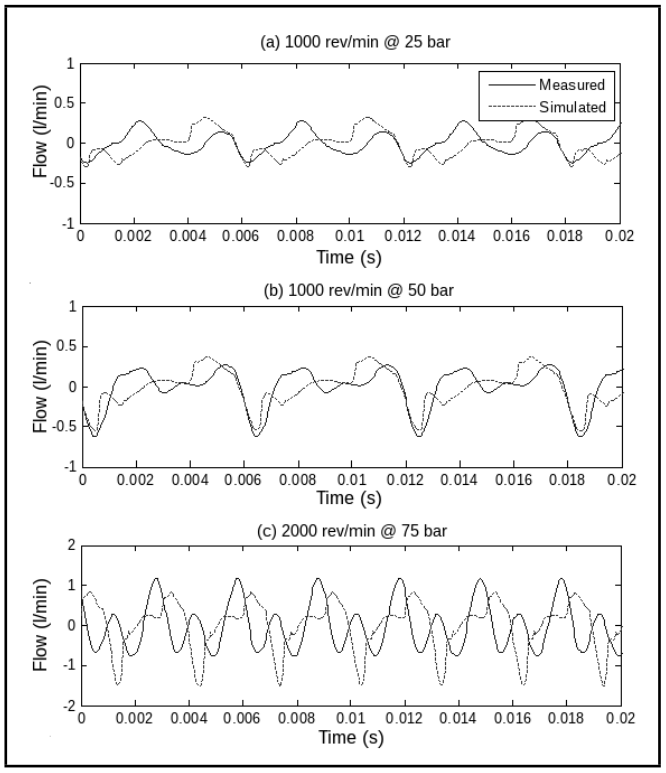

Figure 7. Results of the measured and simulated outlet flow ripple in the time-domain.

run at 1000 rpm and 50 bar. From these results it can be observed that:

1. Excepting the effects of the dynamic flow characteristics, represented in the plot by "spills" along the curve (pointed), the outlet flow (without leakage and vanes flows) is not uniform. In fact, the final signal shape is quite similar to a saw-tooth wave, as can be seen in Fig. 10.

2. There is a 36° lag between the start of two consecutive fluid chamber flows. Also, 88° is the total angular length that the fluid chamber passes over to the discharge port, i.e., the discharge port is opened to a fluid chamber during a rotation of 88° degrees.

In addition, it can be shown that, independent of the intersection point between two consecutive fluid chamber flows, the outlet flow will always exhibit a saw-tooth shape with different amplitudes. In Fig. 11, we can observe some interesting intersection points.

5.2. Under-vane Flow Analysis

As described by Eq. (7), if the compressibility effect is ignored, the under-vane flow will be proportional to the vane radial velocity. The total pump flow ripple caused by under-vane flows will be the sum of all under-vane flow contributions along the rotor revolution, as described by Eq. (8). Figure 12 shows each under-vane flow contribution, while Fig. 13 shows the pump under-vane flow, that is to say, the sum of them.

From the figures it is possible to notice the following:

1. The flow ripple caused by the under-vane flows is not null.

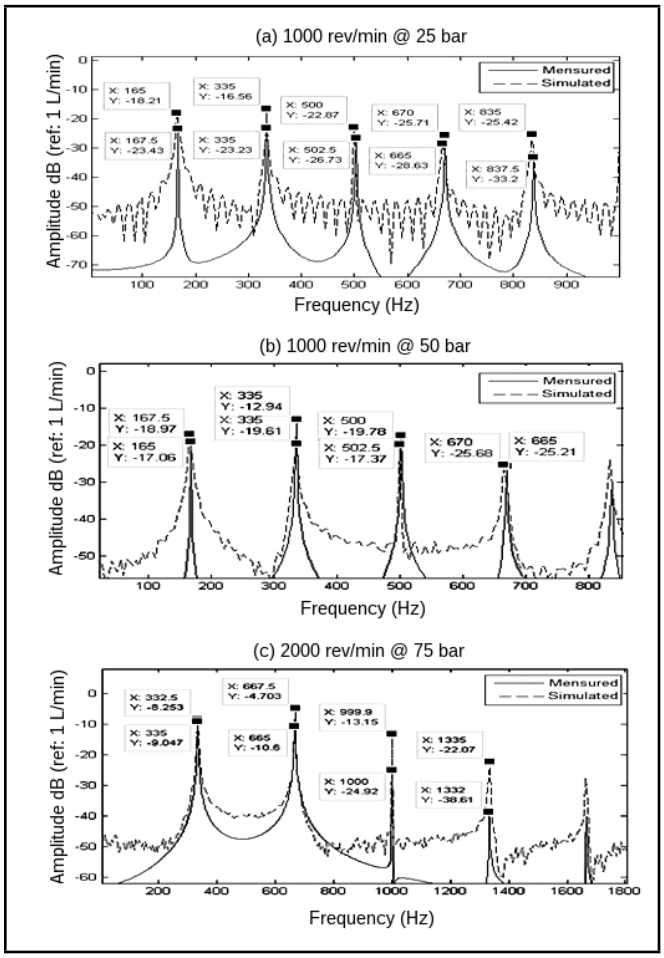

Figure 8. Results of the measured and simulated outlet flow ripple in the frequency-domain.

In fact, its contribution is very significant to the pump outlet flow ripple.

2. In Fig. 12, the upward slope is different than the downward slope. This is due to the fact that the rising and descending parabolic curve length (that, when joined, describes the cam ring suction and the discharge cam ring shape) are not the same. In other words, the intersection point of both parabolic curves is not in the middle of the suction/discharge total path.

3. Besides the triangular shape, the under-vane flow has a steady value along its curve. This is due to a pre-compression zone present in the cam ring shape.

5.3. Compressibility Effect Analysis

Although the hydraulic oil compressibility is very low, large temperature and pressure variations present in the fluid chamber during the pump operation can produce significant fluid compressibility variations. The air dissolved in the fluid is also an important factor that contributes to these variations.

The fluid compressibility affects directly the outlet pump flow ripple and its effect is better seen when the fluid chamber opens to the discharge port; at that moment, a large increase in pressure is applied to the fluid chamber causing outlet flow spills. The amplitude of these spills depends on the

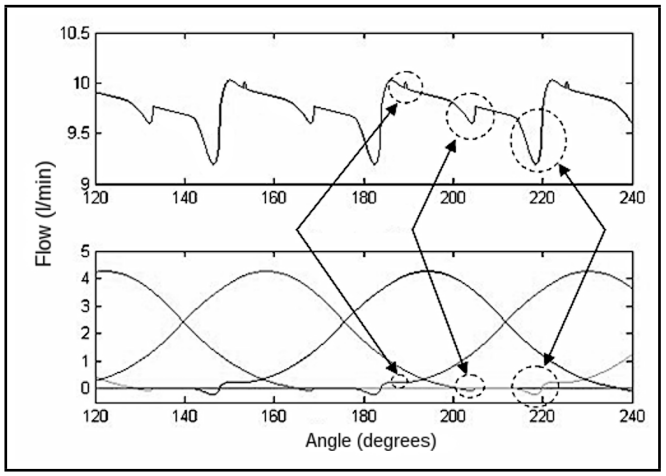

Figure 9. The simulated outlet flow without the influence of the internal leakage flows (upper plot) and the under-vane flows (lower plot), run at 1000 rpm and 50 bar.

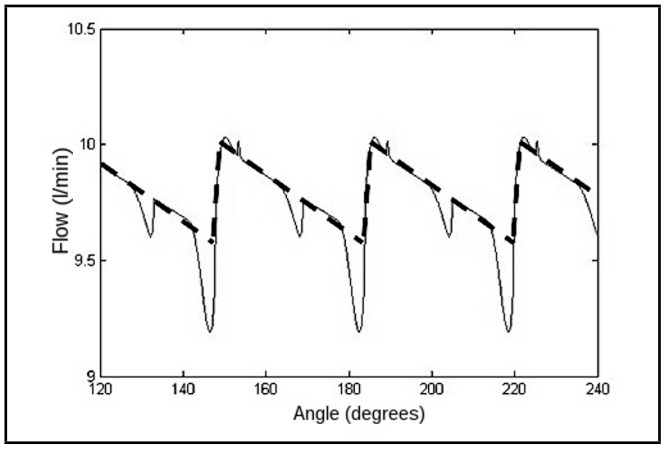

Figure 10. The flow ripple shape, similar to a saw-tooth wave.

fluid compressibility that, mathematically, can be represented by the fluid effective bulk modulus (β_e).

Figure 14 shows the pump outlet flow without the leakage and the under-vane flow contributions, when the fluid effective bulk modulus is varied.

The results presented in Fig. 14 show that some spills amplitude increase when the fluid bulk modulus decreases, thus increasing the outlet flow ripple. However, other regions of the curve are not affected by the bulk modulus variation and, therefore, are not related to the fluid characteristics. These regions are shaped by the geometrical rotating group characteristics.

5.4. Internal Leakage Analysis

The rotating group internal leakage contribution has also been evaluated. Figure 15 shows the outlet flow with and without the leakage contributions. It can be observed that the overall amplitude has decreased when the leakages are taken into account, but the shape of the outlet flow remains roughly the same. In other words, the outlet flow ripple amplitude is not significantly increased when the leakages are considered even though the overall flow amplitude decreases.

These results are valid for the leakages found in the regular pump design from the regular rotating group drawing tolerances. Beyond these values, the leakage effect must be re-

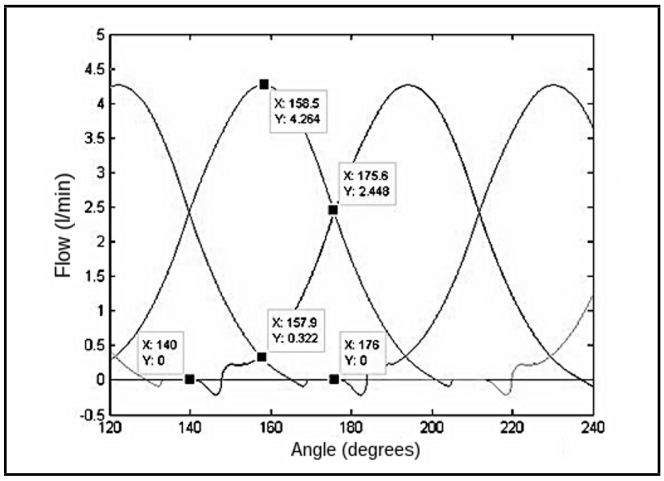

Figure 11. Consecutive fluid chamber flows and some intersection points.

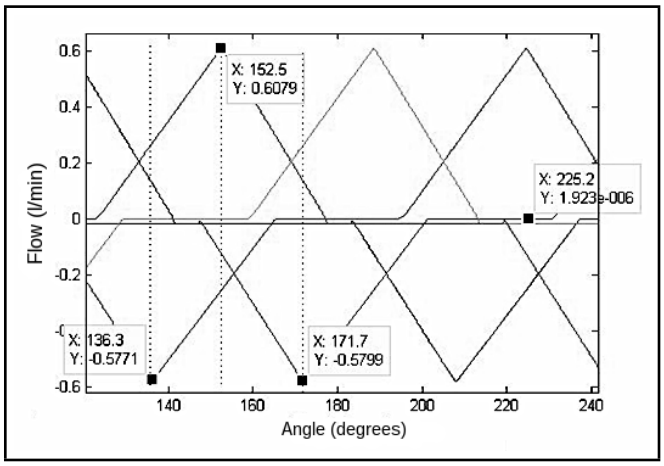

Figure 12. The results for the flow under each of the 10 vanes.

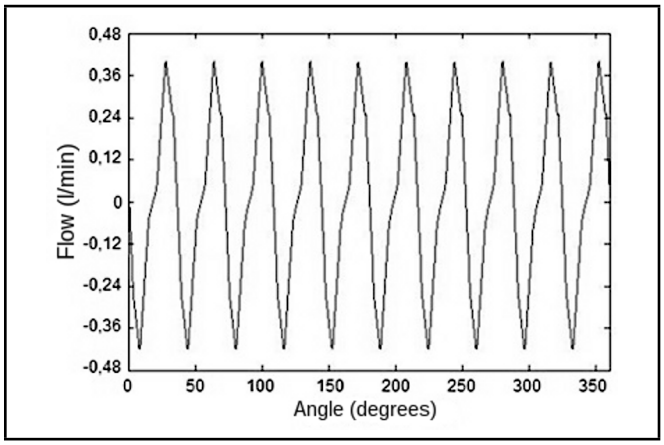

Figure 13. The results of the total pump under-vane flow.

viewed. Previous research[13] has shown the influence of the rotor leakage when the gap between vane and rotor slots increases beyond the drawing tolerances. In that case, the internal leakages have a large influence on the outlet flow.

6. NEW PUMP ROTATING GROUP

From the regular pump flow ripple analysis, a new rotating group design is proposed, aiming at the reduction of the outlet flow ripple amplitude. The new design is based on the follow-

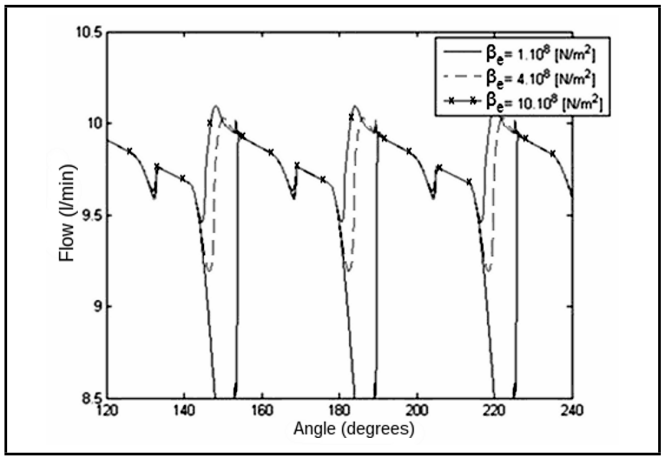

Figure 14. The outlet flow without leakage and the under-vane flows for different values of the fluid effective bulk modulus (1000 rpm at 50 bar).

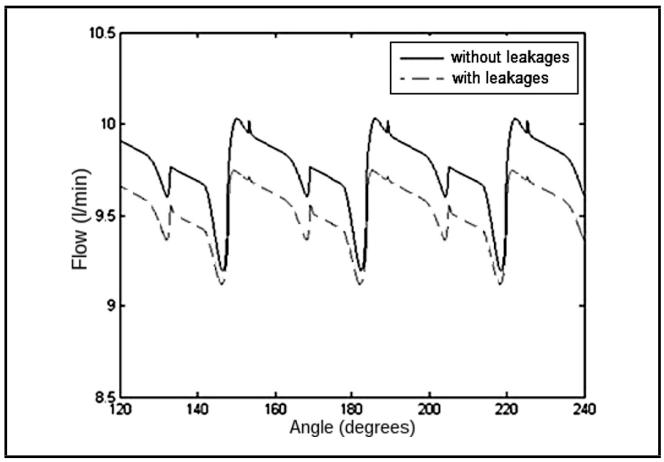

Figure 15. The effect on the outlet flow with and without the internal leakages influence (1000 rpm at 50 bar).

ing modifications:

1. Rotating group for eight vanes.

2. Discharge and suction ports with same angular length found between two consecutive vanes, i.e., 360°/number of vanes. Thus, the beginning of a fluid chamber discharge flow will coincide with the maximum amplitude of a consecutive/trailing fluid chamber discharge flow, making the outlet flow, which is the sum of all fluid chamber flows, roughly steady (plane wave).

3. The intersection point of the parabolas that form the cam ring rising/decreasing shape occur in half of the length; thus, all parabolas that consist of those cam ring variations would have the same length.

4. Cam ring design modification that ensures that when a vane hits the beginning of a suction zone (first rising parabola) some other vane hits, at the same time, the beginning of a discharge zone (first decreasing parabola). In other words, the suction port opening must occur at the same time the discharge port opens. These mechanisms, working together with item 3, ensure that there always will be a pair of under-vane flows that will cancel each other, i.e., flows will have the same shape and am-

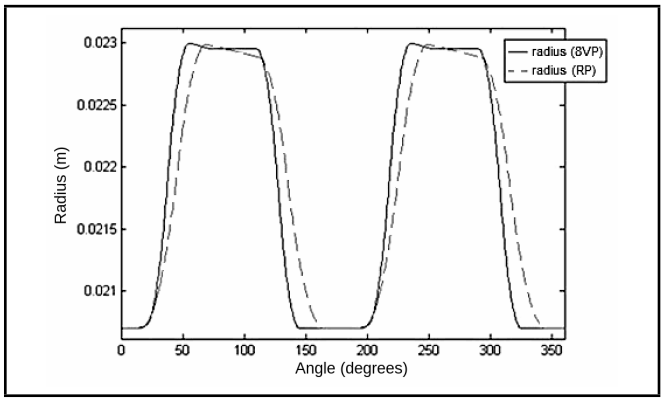

Figure 16. The cam ring profile for the regular pump (RP) and the eight-vane pump (8VP).

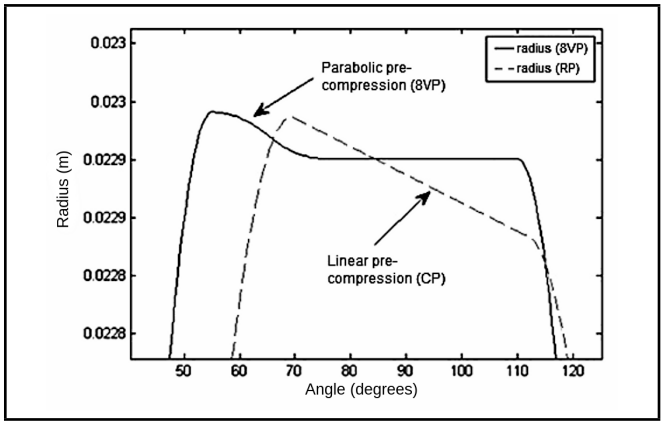

Figure 17. Details of the pre-compression zones for the regular pump and the new pump.

plitude, but in opposite directions. Thus, the total under-vane flows, which are the sum of each under-vane flow, will be, theoretically, equal to zero.

5. To reduce the fluid compressibility effects, a parabolic pre-compression zone (formed by two parabolas, one positive and other negative) is added to the cam ring profile, positioned at the end of the suction zone. To keep the under-vane flow cancellation (as described in items 3 and 4), a parabolic decompression zone is created, formed exactly with opposite pre-compression zone parabolic shape, i.e., negative and positive, respectively, positioned at $360/N_v$ before that one. Thus, the fluid can be pre-compressed prior to the discharge port without disturbing the under-vane flow balance achieved.

It is important to say that this new pump rotation group design is independent of the number of vanes, i.e., it can be built from different number-of-vanes rotors. Thus, choosing an eight-vane rotor gives the possibility to not only reduce noise but to also decrease the pump costs.

Figure 16 shows the cam ring profiles of the regular pump (RP) and the new eight-vane pump (8VP). The differences between the pre-compression and the decompression zones, located at the beginning of the suction ports, are shown in Figs. 17 and 18, respectively.

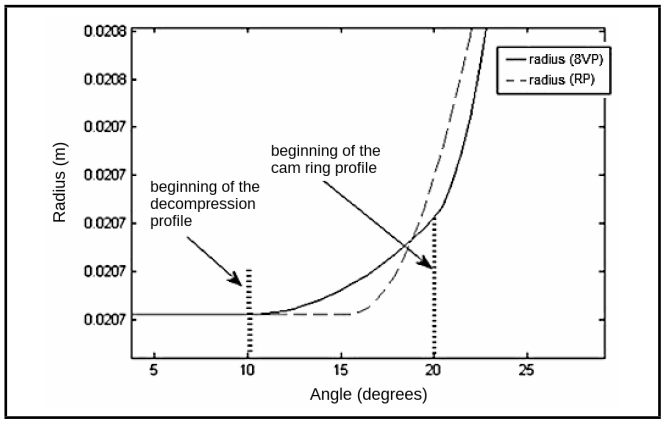

Figure 18. The decompression profile detailing the regular and new cam ring profile.

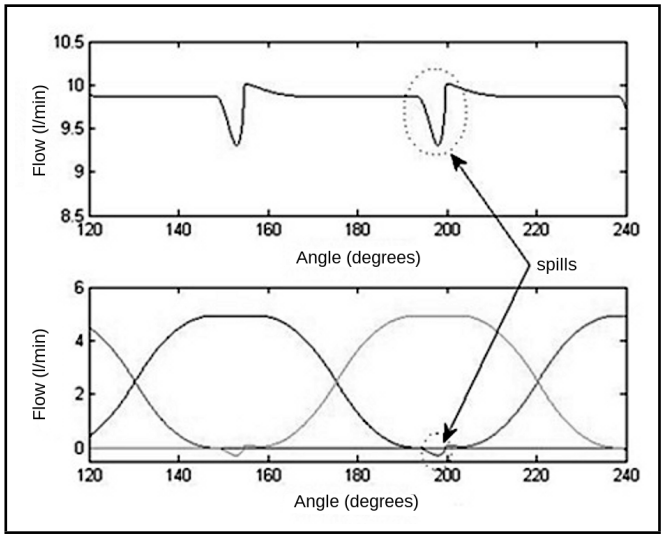

Figure 19. The new pump outlet flow ripple showing spills caused by fluid compression effects.

6.1. Simulation Results

As a consequence of the new rotating group timing, the outlet flow ripple became much more uniform when compared to the current pump one. Figure 19 shows the outlet flow ripple without the under-vane and leakage flows, and the fluid chamber flow packages that forms it. It can be seen that the shape of the outlet flow is planar, although some spills caused by the fluid compression effects are present. For a more realistic result, all flow ripple effects must be taken into account.

As it was discussed previously, the flow ripple caused by internal leakages does not significantly affect the overall pump outlet flow ripple. In fact, even in this new pump design, they show the same unimportant behaviour.

The new flow, under each of the eight vanes, is shown in Fig. 20. Despite very little flow appearings at the beginning of the compression zone, each under-vane flow has its corresponding equal and opposite direction flow, occurring at the same time. It leads the overall under-vane flow (sum of all of them) to be null, as shown in Fig. 21. The peaks present in that figure are just computational precision errors.

Finally, the fluid compression effect is reduced by tuning the pre-compression zone. Several simulations, with different pre-compression amplitudes (changing the slope of the parabola),

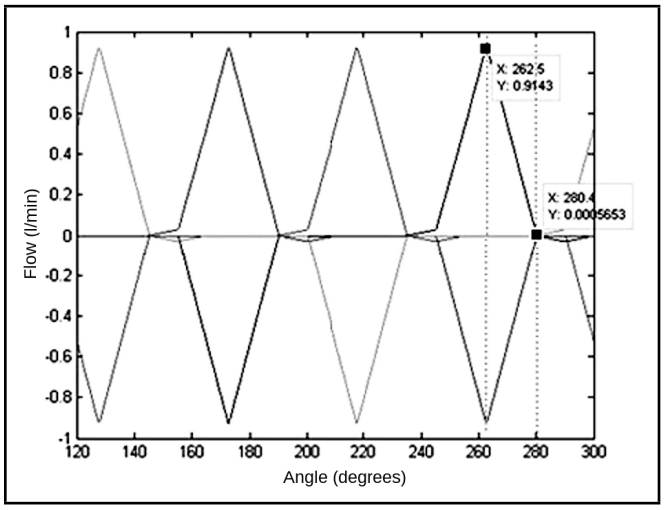

Figure 20. The flow under each of the eight vanes in the new pump design.

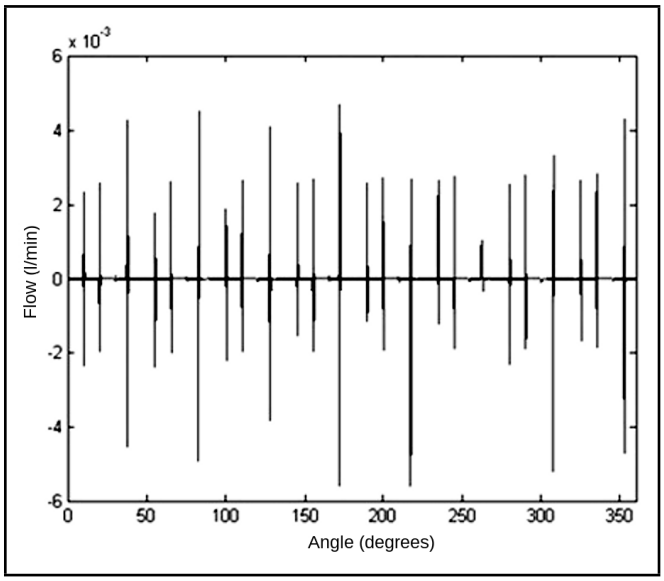

Figure 21. The overall total under-vane flow.

in a large range of bulk modulus values (from 4×10^8 to 14×10^8) was carried out to find the best pre-compression geometric amplitude that produces the lower fluid compression effects (lower flow spill). Once that geometrical value is found, the total outlet flow ripple could be determined. Figure 22 shows the new pump design outlet flow ripple. It can be seen that the flow ripple amplitude was drastically reduced when comparing it with the regular pump one (see Fig. 4).

From the spectral analysis, it can be seen that the new design reduces significantly the outlet flow ripple harmonics amplitude, mainly the lower harmonics, and changes the regular pump frequency pattern. In other words, all the noise harmonic content was shifted down in frequency. This effect, together with the harmonic amplitude reduction, can lead to a significant reduction in the noise observed inside the car.

Figures 23 and 24 show the simulated new pump reduction (in dB) when compared with the regular pump results. Figure 23 shows the results by keeping the rotational speed at 1000 rpm and varying the back-pressure. In Fig. 24, the results are presented, keeping the back-pressure at 50 bar and varying the rotational speed.

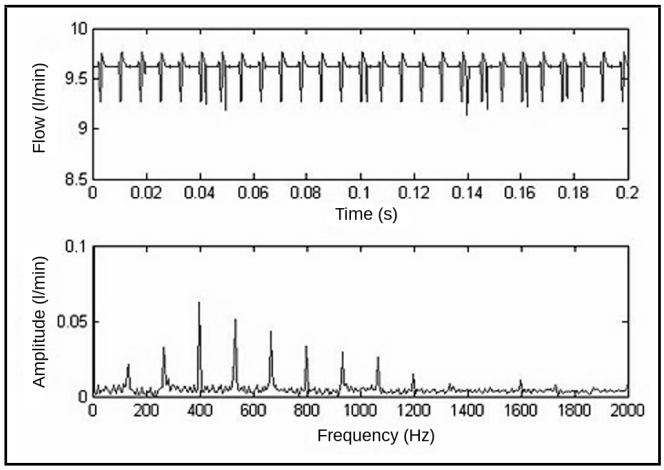

Figure 22. The outlet flow ripple of the new pump in the time and frequency domain.

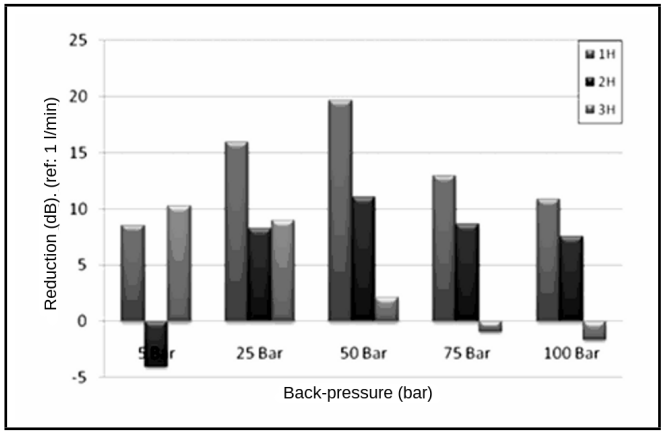

Figure 23. The harmonics amplitude reduction in the new pump design at 1000 rpm for different values of back-pressure.

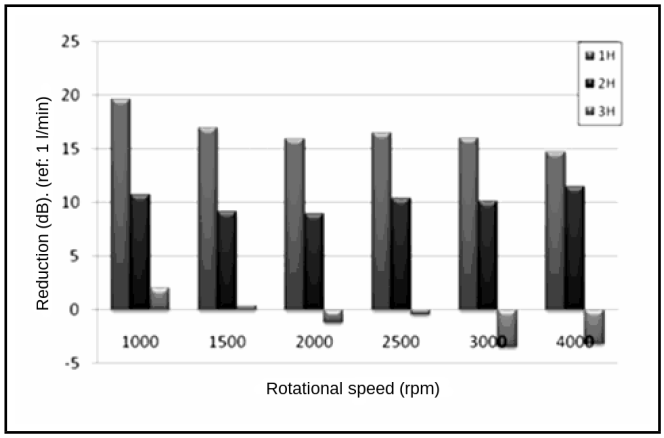

Figure 24. The harmonics amplitude reduction in the new pump design at 50 bar for different rotational speeds.

From the figures, we can observe that the best reduction is achieved when the new pump design is run at 1000 rpm at 50 bar, given an approximate value of flow ripple reduction of 20 dB, 12 dB, and 2 dB at the first (1H), second (2H), and third (3H) harmonic, respectively.

Finally, Figs. 25 and 26 show the details of the proposed new rotating group design.

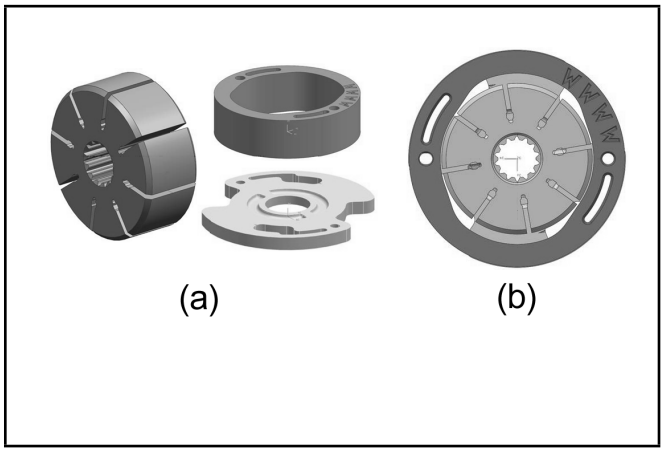

Figure 25. The details of the proposed new rotating group design: a) components, including rotor, cam ring, and thrust plate; and b) assembly.

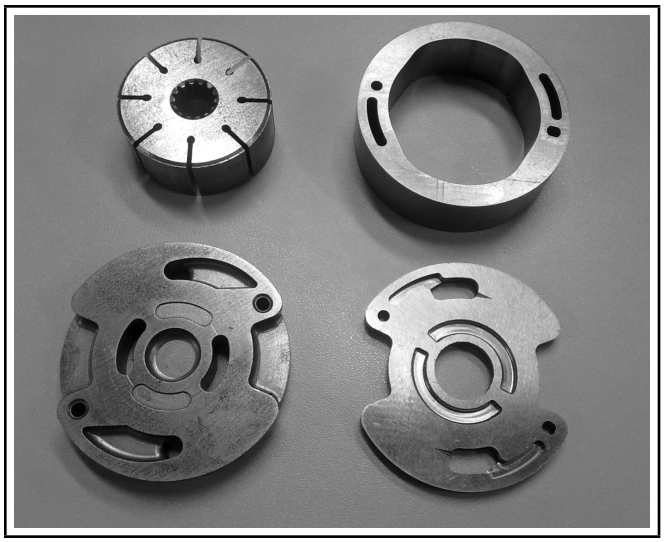

Figure 26. Photograph showing the components of the proposed new pump rotating group.

7. CONCLUSIONS

This work has shown a method to calculate and predict the outlet flow in an automotive positive displacement pump. Additionally, it has presented an experimental method (the secondary source method) to rate the pump flow ripple that was used to validate the numerical results. The main aspects of the pump flow ripple formation were considered and, from this analysis, a new rotating group design has been proposed aiming at the pump outlet flow ripple reduction.

The new rotating group design was simulated and its results were compared with the regular pump ones. The results have shown an excellent outlet flow ripple reduction in a wide range of pump operational conditions. The greatest reduction was achieved for 1000 rpm at 50 bar of back-pressure operational conditions, where the moan noise is perceived[13] to reach almost 20 dB of flow ripple reduction at the first harmonic, and over 10 dB at the second harmonic.

REFERENCES

[1] Zanetti-Rocha, L., Johnston, D.N. and Gerges, S.N.Y. Flow ripple reduction in power steering hydraulic pumps, *Proc. Fluid Power and Motion Control 2010*, Bath, (2010).

[2] Gerges, S.N.Y., Johnston, D.N. and Rocha, L.Z. Noise and vibration in fluid power systems, *Handbook of Hydraulic Fluid Technology*, Taylor & Francis Group, Florida, (2010).

[3] Skaistis, S. *Noise Control of Hydraulic Machinery*, Marcel Dekker, New York, (1988).

[4] Johnston, D.N. Measurement and prediction of the fluid borne noise characteristics of hydraulic components and systems, PhD Thesis, University of Bath, (1987).

[5] Edge, K.A. and Johnston, D.N. The "secondary source" method for the measurement of pump pressure ripple characteristics, part 2: experimental results, *Proc. Inst. Mech. Engrs.—part A*, **204**(1), 41–46, (1990).

[6] ISO 10767-1, Hydraulic fluid power- determination of pressure ripple levels generated in systems and components—part 1: precision method for pumps, International Standardization Organization, Geneva, (1996).

[7] Dickinson A.L., Edge, K.A. and Johnston, D.N. Measurement and prediction of power steering vane pump fluid-borne noise, *SAE Transactions - Journal of Passenger Cars*, **102**(6), 1753–1761, (1993).

[8] Chalu, C. Torque fluctuations and vibrations in a vane pump, Master of Philosophy Thesis, University of Bath, (2004).

[9] Yang, M. Modelling and analysis of pressure pulsations in hydraulic components and systems with particular reference to pump fault diagnosis, PhD Thesis, University of Bath, (2009).

[10] Edge, K.A. and Johnston, D.N. The "secondary source" method for the measurement of pump pressure ripple characteristics, part 1: description of method, *Proc. Inst. Mech. Engrs.—part A*, **204**(1), 33–40, (1990).

[11] BS 6335:1990, *Methods for determining pressure ripple levels generated in hydraulic fluid power systems and components, part 1: secondary source methods for pumps*, British Standards Institution, London, (1990).

[12] Johnston, D.N., Drew, J.E. Measurement of positive displacement pump flow ripple and impedance, *Proc. Inst. Mech. Engrs.—Part I*, **210**(1), 65–74, (1996).

[13] Rocha, L.Z., Paul, S., Jordan, R. and Gerges, S.N.Y. Sound quality evaluations of hydraulic pumps, SAE paper 2008-36-0583, So Paulo, Brazil, (2008).